Semiconducting Cu-doped AlO_x films fabricated by drop-photochemical deposition

Masanari Umemura[1),2)], Masaya Ichimura[1)]

1) Department of Electrical and Mechanical Engineering, Nagoya Institute of Technology, Gokiso, Showa, Nagoya 466-8555, Japan

2) Corresponding Author: Tel. : +81-80-4651-0699, e-mail : 29413039@stn.nitech.ac.jp

Abstract

Cu-doped aluminum oxides (AlO_x) thin films were deposited by the drop photochemical deposition method using an aqueous solution containing $Al(NO_3)_3$, $Cu(NO_3)_2$ and $Na_2S_2O_3$. After deposition, the films were annealed at 400ºC for 60 min. The Cu-doped AlO_x films showed p-type photoresponse in a photoelectrochemical measurement. Moreover, while negligible electrical conductivity was detected for non-doped AlO_x on an insulating substrate, electrical conduction was clearly observed for the Cu-doped films with resistivity of the order of 10^8 Ωcm. The junction between non-doped AlO_x and Cu-doped AlO_x showed rectification and thus was considered to be a p-n junction. Thus, the conductivity and conduction type of aluminum oxide was controlled by Cu doping.

Keywords

Aluminum oxide, semiconductor, Cu doping, photochemical deposition, p-n junction

1. Introduction

α-Al_2O_3 has a wide bandgap of about 8.8 eV and has been used as an insulating ceramic and a substrate material for GaN [1,2]. Amorphous AlO_x films also have high optical transparency, high chemical stability, and high electrical resistivity. By utilizing those properties, AlO_x films have been used in many applications as an insulating film [3-5], a passivation coating [6-8], a protective film [9], biosensor [10], and superlattice for light emitting device [11]. Thus, to date, aluminum oxide has been used as an insulator and has not been used as a conductor, except for application to a resistive switching memory [12, 13]. On the other hand, Ga_2O_3 has been extensively investigated as a wide-gap semiconductor promising for various electronic and optoelectronic devices, and In_2O_3 is widely used as a transparent conductive oxide (TCO). The successful application of these materials can be attributed to successful valence control by the impurity doping. Thus, if the conductivity of aluminum oxide can be controlled by impurity doping, aluminum oxide will also be used as a (semi)conductor in electronics applications [14].

Many fabrication methods of AlO_x have been reported including chemical vapor deposition [15-17], atomic layer deposition [18, 19], pulse laser deposition [20, 21], spray pyrolytic deposition [22], electrochemical deposition (ECD) [23], photochemical deposition (PCD) [24]. Among those methods, PCD and ECD have industrial advantages such as low cost and short manufacturing time. In addition, PCD can fabricate films on insulator substrates including glass. In this paper, we report fabrication of conductive Cu-doped amorphous AlO_x films by drop-photochemical deposition (d-PCD).

In PCD, chemical reactions are activated in the deposition solution by UV irradiation. The PCD reactions of AlO_x are considered to be as follows [24].

$$2S_2O_3^{2-} + h\nu(UV) \rightarrow S_4O_6^{2-} + 2e^- \quad (1)$$

$$S_2O_3^{2-} + h\nu(UV) \rightarrow SO_3^{2-} + S \quad (2)$$

$$Al^{3+} + \frac{3}{2}S + 3e^- \rightarrow AlS_{\frac{3}{2}} \quad (3)$$

$$AlS_{\frac{3}{2}} + \frac{3}{2}H_2O \rightarrow \frac{3}{2}H_2S + AlO_{\frac{3}{2}} \quad (4)$$

$Na_2S_2O_3$ acts as a reduction agent and source of sulfur under UV irradiation. Aluminum sulfide is once formed and then reacts with water to become oxide. We attempt Cu doping in this study. Cu is a potential acceptor element, and in fact, Cu is known to act as an acceptor in oxides and sulfides [25-28]. In addition, ternary compound $CuAlO_2$ is a TCO material with p-type conductivity [29]. Thus, one may suppose that Cu can act as an acceptor in aluminum oxide [14]. It was reported that Cu_xS can be deposited by PCD [30], and thus, Cu atoms will be introduced into the deposited film if Cu ions are added to the deposition solution of AlO_x.

In this work, we first confirm p-type conductivity of Cu-doped AlO_x, and then we fabricate p-n junctions consisting of non-doped and Cu-doped AlO_x.

2. Experimentals

AlO_x thin films were deposited onto fluorine-doped-tin oxide (FTO) coated glass substrate and alkali-free glass substrate. The alkali-free glass substrate was used for the resistivity measurement. Before the deposition, the substrates were washed with acetone and pure water for 5 minutes by ultrasonic cleaning. The deposition solution for non-doped AlO_x contained 10 mM $Al(NO_3)_3 \cdot 9H_2O$ and 50 mM $Na_2S_2O_3$, and the pH of the solution was not adjusted (about 3.6-4.2). For Cu-doped AlO_x deposition, 1, 5, or 10 mM $Cu(NO_3)_2 \cdot 3H_2O$ was added to the solution.

The schematic of d-PCD is shown in Fig. 1. The deposition process was performed by dropping 0.2 mL solution onto the substrate masked with 1.8×1.8 cm^2 deposition area. Then, the solution was irradiated with an ultra-high-pressure mercury lamp with 500 mW/cm^2 irradiation power. Because the dropped solution becomes hazy by the reactions via photo

excitation, after 5 min irradiation, the substrate was washed and dried, and then the solution was dropped again. By repeating the process 10 times, non-doped and Cu-doped AlO_x thin films were fabricated. After the deposition, the thin films were annealed at 400ºC for 60 min. Oxygen vacancy is expected to be a donor-type defect, and therefore, to enhance p-type conduction, the oxygen vacancy concentration should be reduced. Thus, Cu-doped films were annealed in air. On the other hand, non-doped films were annealed in nitrogen to enhance n-type conductivity. For fabrication of the Cu-AlO_x/AlO_x junctions, first the non-doped AlO_x was deposited on the FTO substrate and annealed in nitrogen at 400ºC for 60 min. Then Cu-doped AlO_x, was deposited onto the annealed non-doped AlO_x. Finally, the sample was annealed in air at 400ºC for 60 min.

The compositional analysis of the fabricated films was performed by Auger electron microscope (AES) measurement using the model JEOL JAMP 9500F Auger microprobe at probe current of 2×10^{-8} A and acceleration voltage of 10 kV. For cleaning of film surface, an argon-ion etching was employed. The elemental composition was calculated using literature values of relative sensitivities of elements [31]. Scanning electron microscope (SEM) images were taken with the magnification of 5000 by using JAMP 9500F. The optical transmittance measurement was performed by using the JASCO U-570 UV/VIS/NIR spectrometer with the substrate as the reference. To investigate the conduction type, photoelectrochemical (PEC) measurement was carried out in a three-electrode-system with an Ag/AgCl reference electrode. 0.1 M Na_2SO_4 aqueous solution was used as the electrolyte. For optical excitation, 100 mW/cm^2 light from an ABET technologies 10500 solar simulator was irradiated intermittently with intervals of 5 s while the potential of the sample was swept within a range from -0.5 to 0.5 V with the scanning rate of 5 mV/s. To investigate resistivity and junction properties of the thin films, current-voltage (I-V) measurement was performed for the films on the alkali-free glass substrate and the junction samples on the FTO substrate.

For the I-V measurement of the films fabricated on the insulating glass, indium inter-digit electrodes, whose schematics is shown in Fig. 2, were fabricated by vacuum evaporation. On the others hands, for the measurement of the junctions on the FTO substrate, 1×1 mm^2 indium electrodes were fabricated on the second layer (Cu-doped AlO_x), and the I-V measurement was performed between the In electrode and FTO substrate.

3. Results and discussion

The films thickness is about 0.1 - 0.2 μm for both the non-doped and Cu-doped films. Figure 3 shows the AES spectra of the annealed thin films. The non-doped film is composed of O and Al, and small amount of S was also detected. The composition ratio O/Al was 1.31, below the stoichiometric composition ratio (1.5). The S/Al ratio was about 0.01. The Cu signal was also detected for the Cu-doped AlO_x films deposited with $Cu(NO_3)_2$ concentrations of 5 and 10 mM, but the Cu signal was below detection limit for $Cu(NO_3)_2$ concentrations of 1 mM. Figure 4 shows the elemental composition ratio of the annealed non-doped and Cu-doped AlO_x films calculated from the AES spectra. With increasing $Cu(NO_3)_2$ concentration, the O/Al and Cu/Al ratios were increased. Cu/Al ratio is about 0.04 for $Cu(NO_3)_2$ concentration of 5 mM. O/Al ratio greater than 1.5 could be due to inclusion of other oxides, e.g., CuO and Cu_2O.

Figure 5 shows the SEM images of the annealed non-doped and Cu-doped AlO_x films. From the SEM images, the surface of the non-doped AlO_x thin films was uniform. For the Cu-doped AlO_x thin films, the surface roughness became larger than for the non-doped AlO_x thin films. For all of the thin films, any crack was not found on the surface.

Figure 6 shows the optical transmittance of the annealed non-doped and Cu-doped AlO_x films deposited on the FTO substrate. The non-doped thin films had high transmittance (82~102 %) in a visible wavelength region. (We used the FTO substrate as the reference in

the transmission measurement, and the transmittance of the FTO substrate has a wave pattern due to the interference effects. The interference pattern was modified, i.e., the top and bottom positions were shifted, with the film deposited on it. Therefore the transmission can exceed 100 %.) The gradual decrease in transmittance between 300 and 1000 nm could be due to light scattering by roughness of the thin film surface. By Cu doping, the transmittance was overall decreased slightly, which is probably due to increasing surface roughness.

Figure 7 shows the PEC measurement results of the annealed non-doped and Cu-doped AlO_x films. If the sample is an n-type semiconductor, positive photocurrent is observed during the positive potential sweep. If the sample is p-type semiconductor, negative photocurrent is observed. For the non-doped film and the Cu-doped film with $Cu(NO_3)_2$ concentration of 1 mM, photoresponse was not clearly observed. In contrast, Cu-doped AlO_x showed clear p-type photoresponse when the $Cu(NO_3)_2$ concentration is 5 and 10 mM. Thus, doped Cu acts as an acceptor in AlO_x and converts the conduction type to p-type.

Figure 8 shows the I-V measurement results of the annealed non-doped and Cu-doped AlO_x films on the alkali-free glass. (All the I-V curves showed slight positive current for zero applied voltage. That current component would be an offset current generated in the ampere meter and measurement circuit. The current of the non-doped AlO_x film would dominantly be the offset current, which does not depend on bias.) There was no detectable current flow for the non-doped films. On the other hand, the Cu-doped AlO_x thin films had conductivity, and the resistivity calculated from I-V data is plotted in Fig.9. There is scatter in the data among the electrodes fabricated on each sample, but one can see that the resistivity is of the order of 10^8 Ωcm. (We did not perform other measurements such as the Hall measurement, because the resistivities were too high.) In previous reports, the Al_2O_3 thin film's resistivity ranged from 10^{10} to 10^{16} Ωcm [32-34]. Thus, the resistivity of our Cu-doped AlO_x films was lower than the previously reported values by several orders of magnitude. The significant

dependence on the $Cu(NO_3)_2$ concentration was not found. At present, it is not understood why the resistivity did not show clear dependence on the Cu content in the film.

Figure 10 shows the I-V measurement results of the junction between non-doped and Cu-doped AlO_x films on the FTO substrate. Rectification properties were observed for the junction fabricated with the $Cu(NO_3)_2$ concentration of 5 mM. We confirmed that the single film of non-doped AlO_x and Cu-doped AlO_x on FTO showed the ohmic properties, and therefore the interface of the two films is considered to form a p-n junction. It should be noted that significant vertical conduction (in the thickness direction) was observed even for the non-doped film, although the parallel conduction on the alkali-free glass substrate was not observed for the non-doped film. This would be because the grain boundaries are much less influential for the vertical conduction. In the I-V measurement for the films deposited on FTO, the current flow through the films vertically because FTO is conductive. From the SEM images, the grain size was estimated to be 0.1 - 0.2 μm, which is roughly the same as the film thickness. Thus, in the vertical conduction of the film on FTO, the current does not need to go through many grain boundaries. On the other hands, for the film deposited on the alkali free glass substrate, the current flows parallel to the substrate between 0.2 mm-apart two electrodes. Thus, the current needs to go through many grain boundaries. As a result, the parallel conductance can be much smaller than the vertical conductance. The p-n junction fabricated with the $Cu(NO_3)_2$ concentration of 10 mM showed poorer rectification properties. This could be related to the fact that the excessive Cu doping does not enhance p-type conductivity, as shown in Fig.9.

The results of the present study show that Cu-doped AlO_x is a transparent, p-type semiconducting material. Thus, it is demonstrated for the first time that the conduction type and conductivity of aluminum oxide can be controlled by proper impurity doping. We are now attempting to reduce resistivity by modifying the deposition process.

4. Conclusion

In this study, non-doped and Cu-doped AlO_x thin films were fabricated by d-PCD, and electrical and optical characteristics were investigated. Without Cu doping, the AlO_x film on the glass substrate had negligible electrical conductivity. On the other hands, Cu-doped AlO_x showed p-type photoresponse in the PEC measurement, and its resistivity was of the order of 10^8 Ωcm. The p-n junction between non-doped AlO_x and Cu-doped AlO_x showed rectification. Thus, aluminum oxide can be regarded as another wide bandgap semiconductor having variety of potential applications.

References

[1] French R H 2008 *J. Amer. Ceram. Soc.* **73** 477

[2] Kushvaha S S, Kumar M S, Maurya K K, Dalai M K and Sharma N D 2013 *AIP Adv* **3** 092109

[3] Kim D S, Kim S N, Kim K W, Im K S, Kang H S, Kwak E H and Lee J H 2011 *J. Korean Phys. Soc.* **58** 1500

[4] Ye P D, Yang B, Ng K K, Bude J, Wilk G D, Halder S and Hwang J C M 2005 *Appl. Phys. Lett.* **86** 063501

[5] Fiorenza P, Greco G, Schilirò E, Iucolano F, Nigro R L and Roccaforte F 2018 *Jpn. J. Appl. Phys.* 57 050307

[6] Hoex B, Schmidt J, Bock R, Altermatt P P, van de Sanden M C M and Kessels W M M 2007 *Appl. Phys. Lett.* **91** 112107

[7] Benick J, Richter A, Hermle M and Glunz S W 2009 *Phys. Status Solidi: Rapid Res. Lett.* **3** 233

[8] Richter A, Benick J, Feldmann F, Fell A, Hermle M and Glunz S. W 2017 *Sol. Energy Mater. Sol. Cells* **173** 96

[9] Ghosh A P, Gerenser L J, Jarman C M and Fornalik J E 2005 *Appl. Phys. Lett.* **86** 223503

[10] Asai N, Shimizu T, Shingubara S and Ito T 2018 *Sens. Actuators B Chem.* **276** 534

[11] Oshima T, Kato Y, Kobayashi E and Takahashi K 2018 *J. Appl. Phys.* **57** 080308

[12] Lee J, Nigo S, Nakano Y, Kato S, Kitazawa H and Kido G 2010 *Sci. Technol. Adv. Mater.* **11** 025002

[13] Wu Y, Jou S and Yang P 2013 *Thin Solid Films* **544** 24

[14] Ichimura M *J. Electron. Mater* in press (doi.org/10.1007/s11664-018-6749-9).

[15] Kumagai H, Toyoda K, Matsumoto M and Obara M 1993 *Jpn. J. Appl. Phys.* **32** 6137

[16] Koh W, Ku S J and Kim Y 1997 *Thin Solid Films* **304** 222

[17] Kim D H, Jeong H J, Park J and Park J S 2018 *Ceram. Int.* **44** 459

[18] Higashi G S and Fleming C G 1989 *Appl. Phys. Lett.* **55** 1963

[19] Patsiouras L, Skotadis E, Gialama N, Drivas C, Kennou S, Giannakopoulos K and Tsoukalas D 2018 *Nanotechnol.* **29** 465706

[20] Shi L, Frankena H J and Mulder H 1990 *Vacuum* **40** 399

[21] Boidin R, Halenkovič T, Nazabal V, Beneš L and Němec P 2016 *Ceram. Int.* **42** 1177

[22] Dhongea B P, Mathews T, Sundari S T, Thinaharan C, Kamruddin M, Dash S and Tyagi A K 2011 *Appl. Surf. Sci.* **258** 1091

[23] Haleemab A M A and Ichimura M 2014 *Mater. Lett.* **130** 26

[24] Sato S and Ichimura M 2017 *Mater. Res. Express* **4** 046405

[25] Rahmani M B, Keshmiri S H, Shafiei M, Latham K, Wlodarski W, du Plessis J and Kalantar-Zadeh K 2009 *Sens. Lett.* **7** [4] 621

[26] Ichimura M and Maeda Y 2015 *Thin Solid Films* **594** 277

[27] Ahn K S, Deutsch T, Yan Y, Jiang C S, Perkins C L, Turner J and Jassim M A 2007 *J. Appl. Phys.* **102** 023517

[28] Ingler Jr W B and Khan S U M 2005 *Int. J. Hydrogen Energy* **30** 821

[29] Kawazoe H, Yasukawa M, Hyodo H, Kurita M, Yanagi H and Hosono H 1997 *Nature* **389** 939

[30] Podder J, Kobayashi R and Ichimura M 2005 *Thin Solid Films* **472** 71

[31] Mroczkowski S and Lichtman D 1985 *J. Vac. Sci. Technol.* A **3** 1860

[32] Solanki R, Ritchie W H and Collins G J 1983 *Appl. Phys. Lett.* **43** 454

[33] Fan J F, Sugioka K and Toyoda K 1991 *Jpn. Appl. Phys.* **30** 1139

[34] Fan J F and Toyoda K 1993 *Jpn. Appl. Phys.* **32** 1349

Figure Captions

Fig.1. Apparatus of the d-PCD method.

Fig.2. The schematics of the indium inter-digit electrodes.

Fig.3. AES spectra of the annealed non-doped and Cu-doped AlO_x films.

Fig.4. Composition ratio of the annealed non-doped and Cu-doped AlO_x films calculated from AES spectra.

Fig.5. SEM images of annealed non-doped and Cu-doped AlO_x films.

Fig.6. Optical transmittance of the annealed non-doped and Cu-doped AlO_x films deposited on the FTO substrate.

Fig.7. PEC measurement results of the annealed thin films. (a): non-doped and Cu-doped AlO_x films with $Cu(NO_3)_2$ concentration of 1 mM. (b): Cu-doped AlO_x films with $Cu(NO_3)_2$ concentration of 5 and 10 mM.

Fig.8. I-V measurement results of the annealed non-doped and Cu-doped AlO_x films on the alkali-free glass.

Fig.9. Resistivity of the annealed Cu-doped AlO_x films calculated from I-V measurement results.

Fig.10. I-V measurement results of the annealed heterojunction between non-doped and Cu-doped AlO_x films on the FTO substrate.

Figure 1:

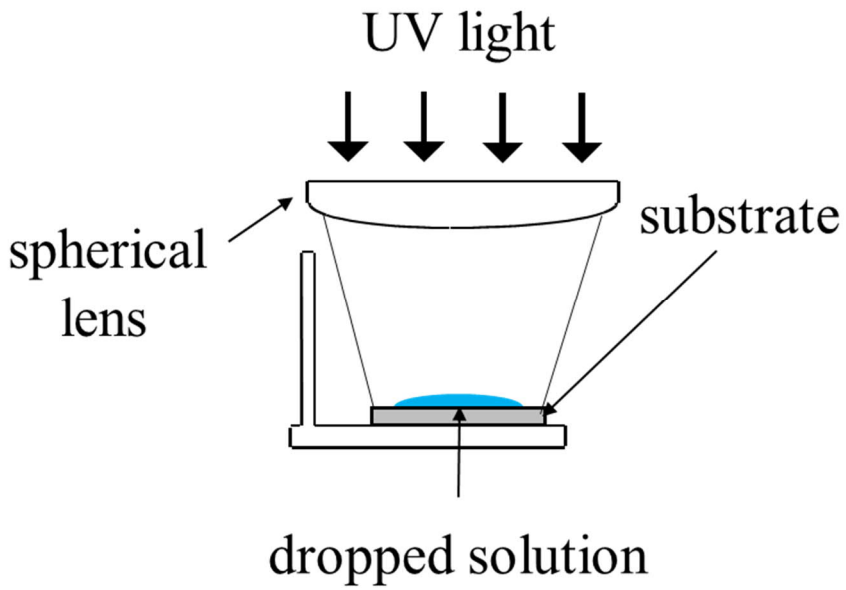

Figure 2:

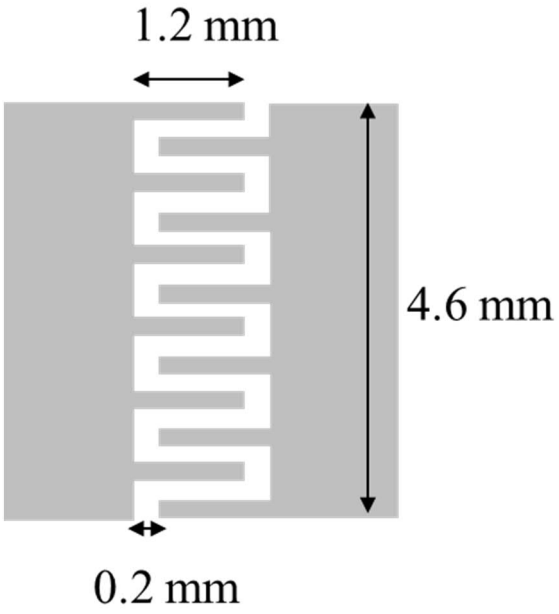

Figure 3:

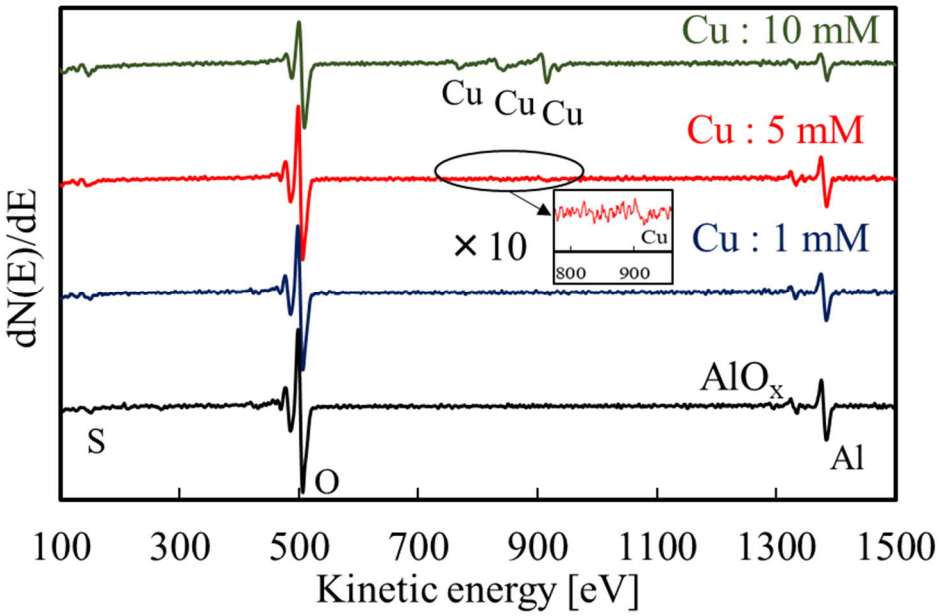
Cu : 10 mM
Cu Cu Cu
Cu : 5 mM
× 10
Cu
800 900
Cu : 1 mM
AlO$_x$
S
O
Al
dN(E)/dE
100 300 500 700 900 1100 1300 1500
Kinetic energy [eV]

Figure 4:

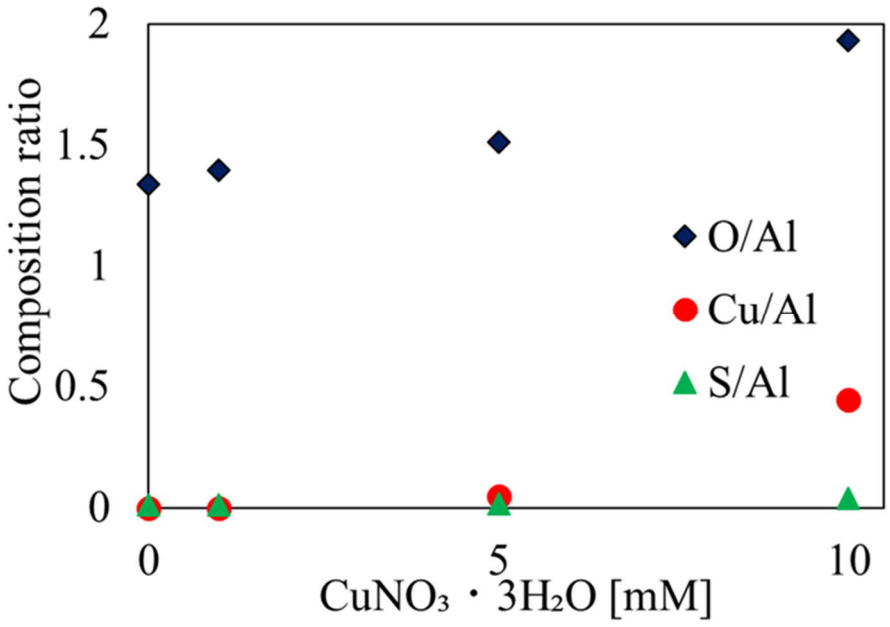

Figure 5:

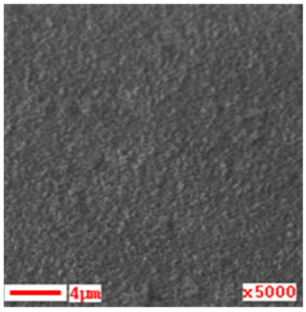

Non-doped films

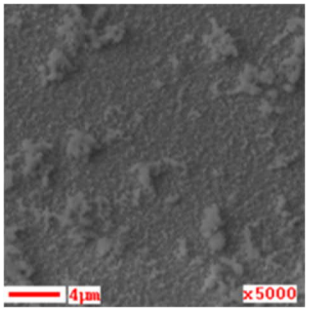

$Cu(NO_3)_2 \cdot 3H_2O$: 1 mM

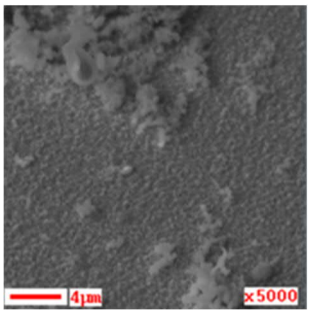

$Cu(NO_3)_2 \cdot 3H_2O$: 5 mM

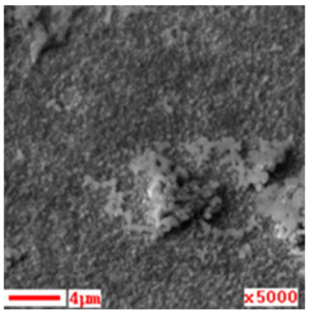

$Cu(NO_3)_2 \cdot 3H_2O$: 10 mM

Figure 6:

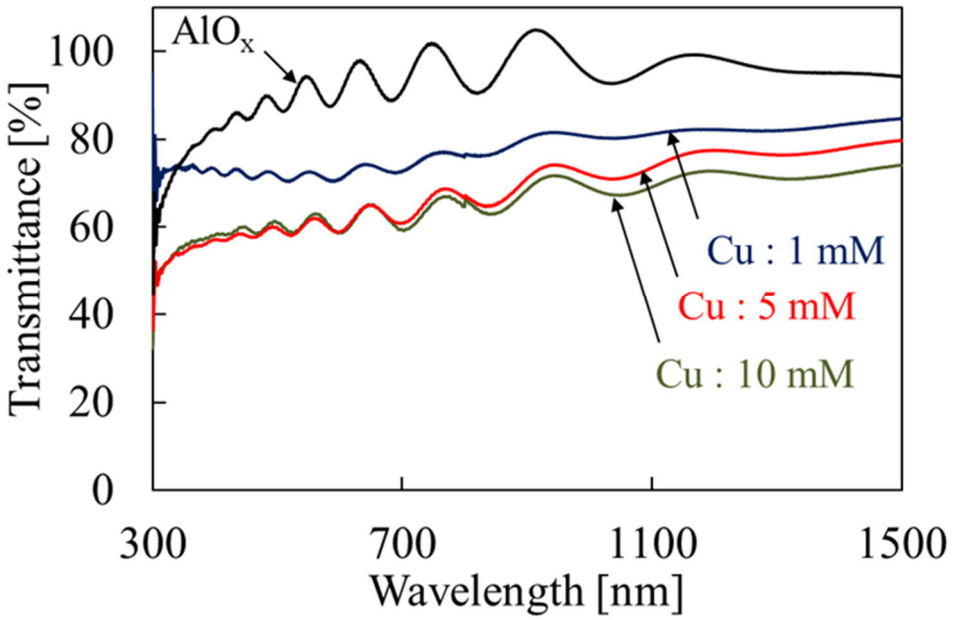
AlOx
100
80
60
40
20
0
Transmittance [%]
300
700
1100
1500
Wavelength [nm]
Cu : 1 mM
Cu : 5 mM
Cu : 10 mM

Figure 7:

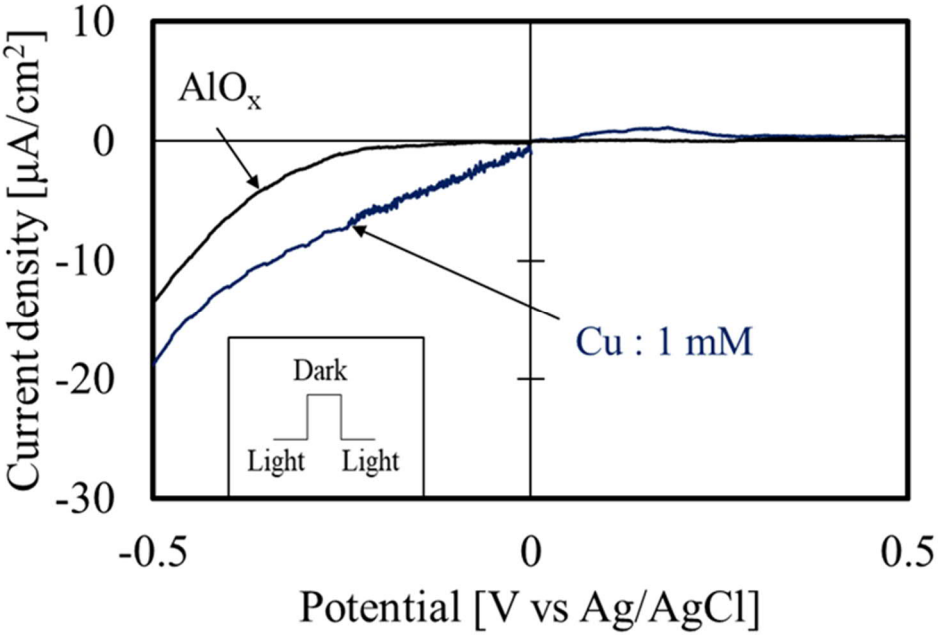

Fig.6(a)

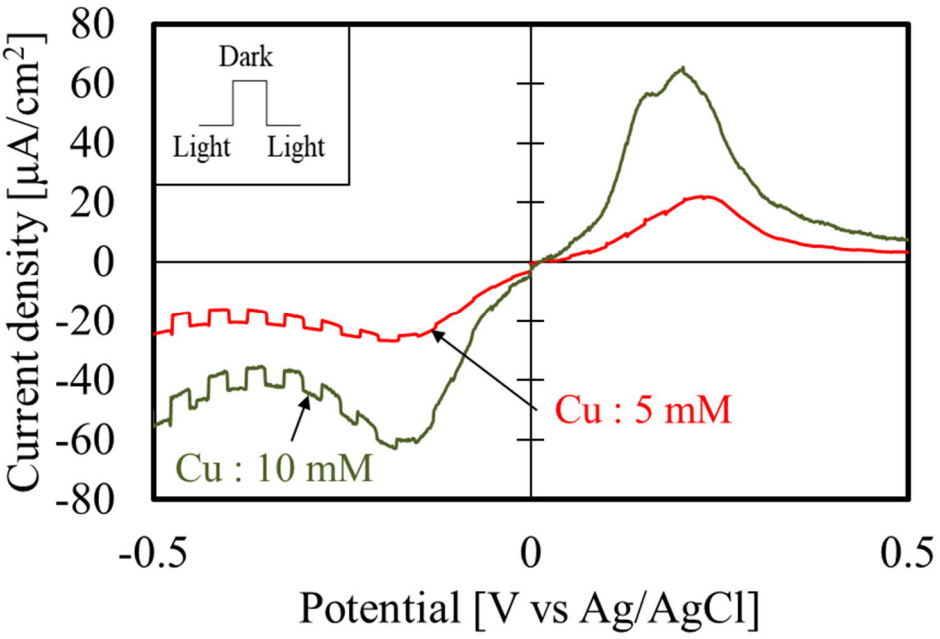

Fig.6(b)

Figure 8:

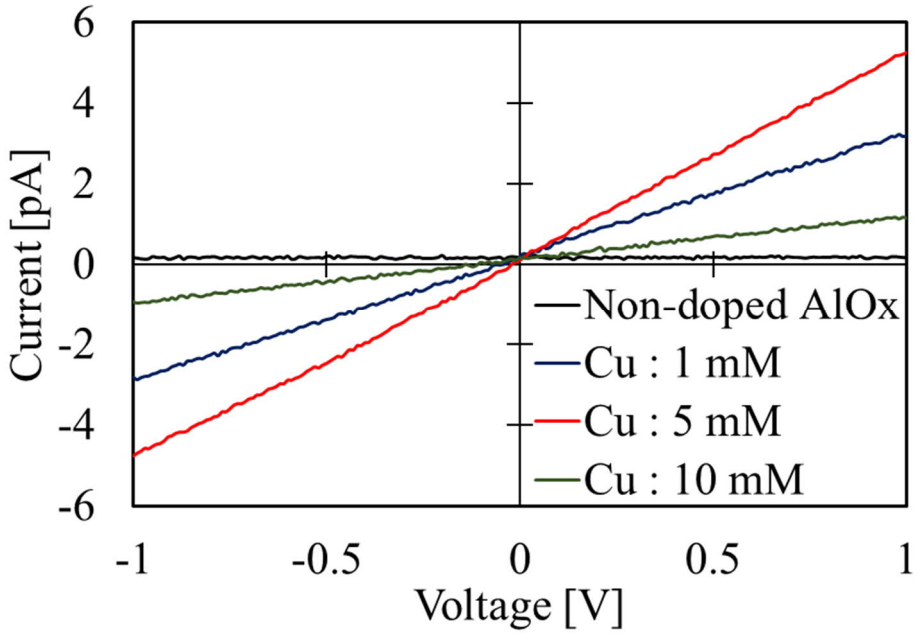
6
4
2
0
-2
-4
-6
Current [pA]
-1
-0.5
0
0.5
1
Voltage [V]
Non-doped AlOx
Cu : 1 mM
Cu : 5 mM
Cu : 10 mM

Figure 9:

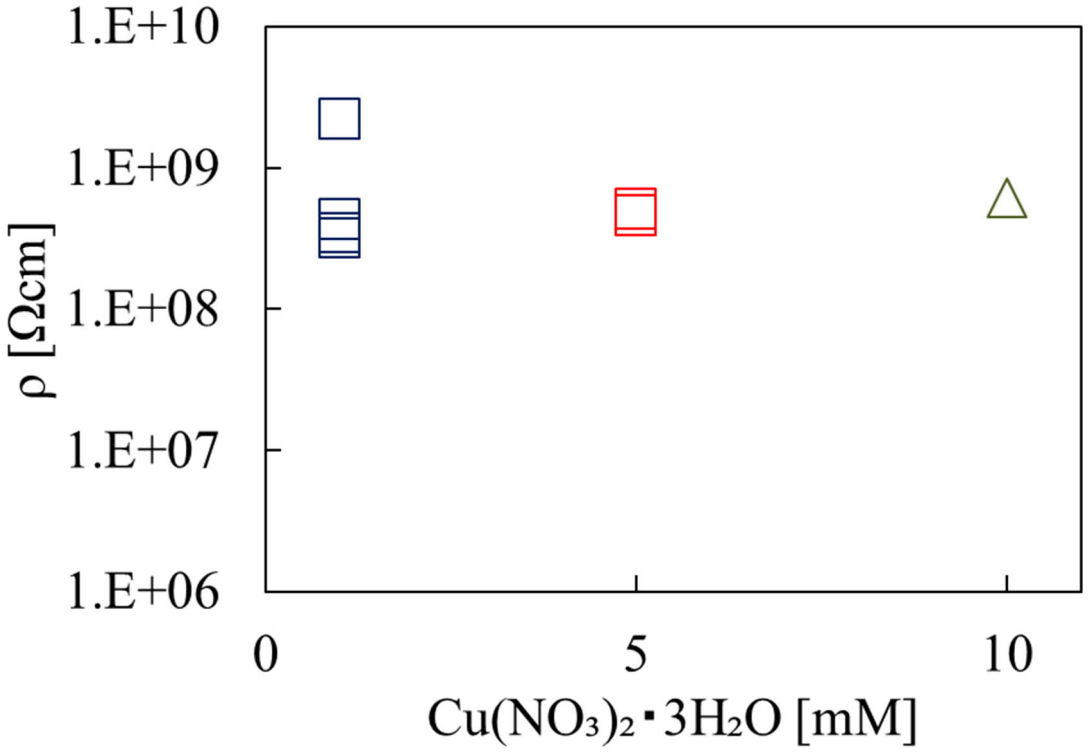

Figure 10:

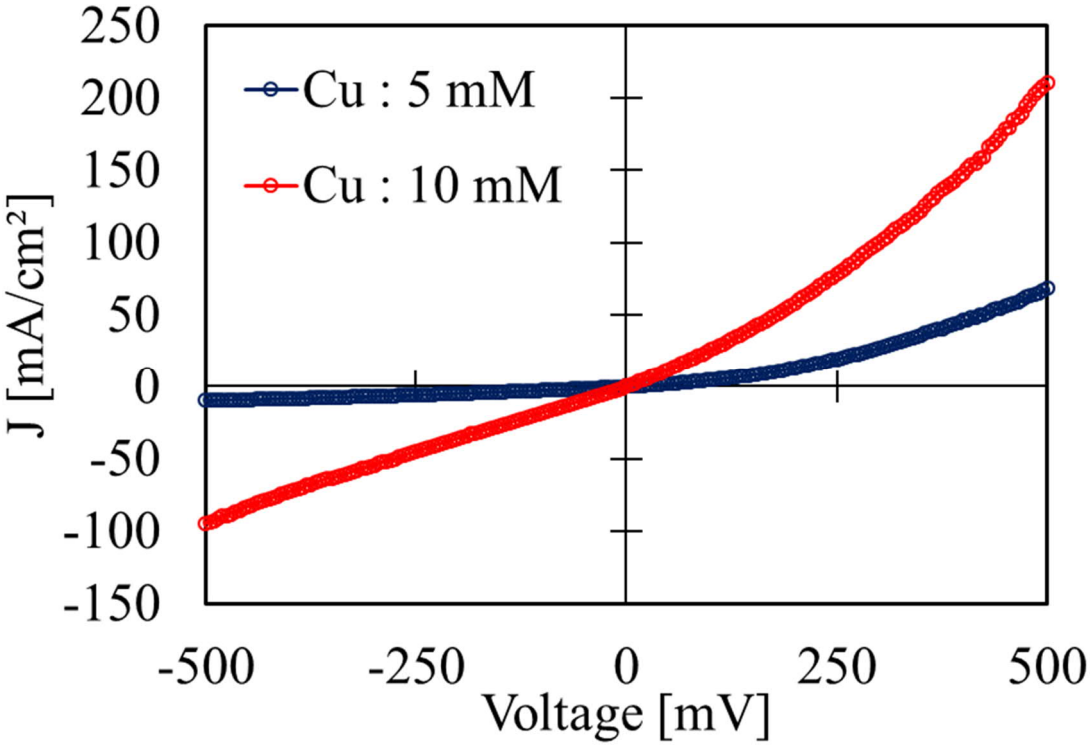
250
200
150
100
50
0
-50
-100
-150
J [mA/cm²]
Cu : 5 mM
Cu : 10 mM
-500
-250
0
250
500
Voltage [mV]